

Probing the spin correlations of $t\bar{t}$ production at NLO QCD+EW

Rikkert Frederix*, Ioannis Tsinikos[†] and Timea Vitos[‡]

Theoretical Particle Physics, Department of Astronomy and Theoretical Physics, Lund University, Sölvegatan 14A, SE-223 62 Lund, Sweden

Abstract

In this work we investigate the NLO QCD+EW corrections to the top quark pair production and their effects on the spin correlation coefficients and asymmetries at fixed-order top quark pair production and LO decay in the dilepton channel, within the narrow-width approximation. The spin correlations are implicitly measured through the lepton kinematics. Moreover we study the EW effects to the leptonic differential distributions. We find that the EW corrections to the $t\bar{t}$ production are within the NLO QCD theoretical uncertainties for the spin correlation coefficients and the leptonic asymmetries. On the other hand, for the differential distributions we find that the EW corrections exceed the NLO QCD scale uncertainty band in the high rapidity regimes and are of the order of the NLO QCD scale uncertainty in the case of invariant mass and transverse momentum distributions.

Contents

1	Introduction	2
2	Theoretical setup	3
2.1	Reweighting in fixed-order PS point generation	4
2.2	Spin correlation coefficients	6
2.3	Asymmetries	8
3	Numerical setup	9
4	Results	9
5	Conclusion and discussion	14

*rikkert.frederix@thep.lu.se

[†]ioannis.tsinikos@thep.lu.se

[‡]timea.vitos@thep.lu.se

1 Introduction

As the heaviest particle in the well-established Standard Model of particle physics, the top quark is of interest for investigation for multiple purposes. Firstly, its role in the fine-tuning problem is exquisite. Secondly, it is a close portal to any beyond Standard Model theories. To make precise predictions for observables related to top quarks is of utmost interest for understanding the present idea of particle physics and to enlarge our views of it by extensions to the existing theories.

After its discovery in 1995, the top quark has been detected in numerous high-energy processes, both in single-top, top quark pair, and production in association with other particles. In pair production, the spin correlation effects serve as a probe for investigation of the underlying physics. Due to its high mass and hence short lifetime, the top quark decays (with almost 100 % branching ratio to Wb) before the spin decorrelation sets in. Thus, the decay products of top quarks carry the spin information and hence provide an optimal source for understanding the nature of top quarks by indirect spin correlation measurements. The prominent decay channel is the all-hadronic channel, in which both the weak bosons decay to quarks. However, the dilepton decay channel (with branching ratio $\sim 10.5\%$) provides a cleaner signature at hadron-hadron collisions and thus an important choice for investigation on the spin correlation effects.

The top quark spin correlations and the differential distributions of the decay products have been previously studied at various levels of precision. The effects of the top quark spin correlations are revealed to the dilepton decay channel. They are studied at NLO QCD accuracy [1–3], at NLOW (NLO QCD + Weak) accuracy [4] and at NLOW through the spin correlation coefficients [5]. The spin correlation coefficients have been compared to experimental data at both ATLAS [6] and CMS [7] collaborations. In the latter case the lepton asymmetries are also presented and furthermore a comparison of the spin-correlated and uncorrelated NLO QCD predictions is done to point out the importance of including the spin correlations in calculations of such observables. A special attention was brought to one observable, $\Delta\Phi_{\ell\ell}$, the angle in the transverse plane of the charged leptons, which was measured by CMS [7] and ATLAS [8] and compared to NLO QCD predictions. This was followed by the NNLO QCD study [9], where the specific observable was found to deviate from the Standard Model predictions in the inclusive (unfolded measurements) region, while fitting nicely to the theory predictions in the fiducial region. The decay product differential distributions for the top quark pair semi-leptonic and leptonic decay are studied at NLO QCD with the top quarks on-shell [10], and including off-shell effects and non-resonant contributions [11, 12]. The dilepton channel is studied including part of the NLO EW corrections [13]. The leptonic differential distributions are also compared to the experimental data in ATLAS [8] and CMS [14]. Recently in Ref. [15], all the aforementioned observables are calculated at NNLO QCD with on-shell top quark decays and the results are compared with experimental data. Despite the high level of accuracy, there are still slight tensions between theory and experiment in the normalised differential distributions, like the $\Delta\Phi_{\ell\ell}$ at the inclusive level, the invariant mass and transverse momentum of the lepton pair, as well as the transverse momentum of the leptons in the fiducial region. The different level of agreement of the $\Delta\Phi_{\ell\ell}$ distribution with the data in the fiducial and the inclusive regime shows that most probably the reason is the use of NLO QCD predictions for the unfolding to the full phase space. This is discussed in detail in Ref. [9]. Furthermore in Ref. [15] it is shown that the tension of this observable with the data in the inclusive phase space persists even after using the expanded definition at NNLO in QCD. Regarding other leptonic distributions (*e.g.* $m(\ell\ell), p_T(\ell\ell)$), slight tensions are shown in Ref. [15] in the ratios of the data w.r.t. the NNLO

QCD predictions in the fiducial phase space.

As no clear explanation to these slight discrepancies between theory and data has yet been found, a natural next step in the investigation within the Standard Model is the inclusion of the full EW effects at NLO to a specific set of observables. In this work we calculate at fixed-order, for the first time, the complete NLO $t\bar{t}$ production followed by the LO top quark pair decays through the dilepton channel in the narrow-width approximation (NWA). We focus our study on the spin correlation coefficients, the leptonic asymmetries and normalised differential distributions. We further explain the reweighting technique, which is used in the decay chain.

The structure of this paper is as follows. In Sec. 2 we introduce the theoretical framework in which we calculate the observables perturbatively, then we introduce the reweighting procedure for fixed-order phase-space points, followed by the spin correlation coefficient and asymmetry definitions. In Sec. 3 we explain our calculational setup and input parameters. In Sec. 4 we present our results for the coefficients and asymmetries, and a set of various distributions in the leptonic kinematics, in all cases comparing NLO QCD and complete-NLO results. Finally, we discuss our results and conclude in Sec. 5.

2 Theoretical setup

The dilepton decay channel of top quark pair production has contributions from non-resonant, single-resonant and double-resonant diagrams. In the NWA, in which the top quarks are produced on-shell, only the double-resonant diagrams are taken into consideration. A full calculation of the dilepton final state $\ell^+\ell^-\nu\bar{\nu}b\bar{b}$ would cover all these contributions to this process. However, the non-double-resonant contributions are expected to be very small for the observables studied in this work, due to the small width-to-mass ratio Γ_t/m_t of the produced top quarks. Within the decay chain, resonant particles are produced on-shell and in a next step are further decayed, in this way compactly implementing the NWA.

Utilising MadGraph5_aMC@NLO [16] and its internal tool for decaying resonant particles, MadSpin [17], one efficiently achieves a fully-decayed set of events. The current version of MadSpin calculates all decays and the corresponding spin correlations at tree-level. Assigning these decays to a set of production phase-space (PS) points from leading-order generation is trivial, as there is no ambiguity in the way the PS points are reweighted. The algorithm for obtaining decayed PS points from a fixed next-to-leading order sample is however currently not yet implemented in the public version of MadSpin. For the current project where the NLO effects, including both the QCD and EW corrections, are included in the production, a method for reweighting fixed-order PS points is developed and utilised.

It should be noted, however, that MadSpin does not handle the virtual corrections in the production PS points and hence these are not included in the spin correlations. To properly describe this, let us first introduce the notation for the perturbative expansions of the process $pp \rightarrow t\bar{t}$. We expand a general observable Σ at fixed-order in the electroweak α and strong α_S coupling constants with the following notation,

$$\begin{aligned} \Sigma_{\text{LO}}(\alpha, \alpha_S) &= \underbrace{\alpha_S^2 \Sigma_{2,0}}_{\text{LO}_1} + \underbrace{\alpha_S \alpha \Sigma_{1,1}}_{\text{LO}_2} + \underbrace{\alpha^2 \Sigma_{0,2}}_{\text{LO}_3} \\ \Sigma_{\text{NLO}}(\alpha, \alpha_S) &= \underbrace{\alpha_S^3 \Sigma_{3,0}}_{\text{NLO}_1} + \underbrace{\alpha_S^2 \alpha \Sigma_{2,1}}_{\text{NLO}_2} + \underbrace{\alpha_S \alpha^2 \Sigma_{1,2}}_{\text{NLO}_3} + \underbrace{\alpha^3 \Sigma_{0,3}}_{\text{NLO}_4} \end{aligned} \quad (1)$$

where the NLO pieces include both the virtual and real corrections. We refer to the leading-order term of LO_1 as LO QCD, the leading-order NLO contribution of LO_1+NLO_1 as NLO QCD and the leading NLO electroweak contribution of LO_1+NLO_2 as NLO EW. In the present work, the NLO QCD+EW refers to the complete NLO, that is, the full $\text{LO}_1+\text{LO}_2+\text{LO}_3+\text{NLO}_1+\text{NLO}_2+\text{NLO}_3+\text{NLO}_4$. Regarding the full process under study we attach the LO leptonic top quark pair decay ($O(\alpha^4)$) to the perturbative orders in Eq. 1.

We extend MadSpin to include decays of fixed-order PS points. MadSpin reads the production LHE file with the fixed-order PS points and re-computes the tree-level matrix element for each PS point including the decay, approximating the virtual diagram contributions with the tree-level ones. Top quark pair production has been also studied at NLO QCD in production and decay within the MCFM framework [18]. We will use this tool to examine the effects of the spin correlations from the virtual NLO QCD part of the $t\bar{t}$ production.

2.1 Reweighting in fixed-order PS point generation

Reweighting in the decay chain approximation from uncorrelated to spin-correlated decays was developed for event generation with parton showering in Ref. [19]. The method is based on relating the differential weight of the fully decayed event to the production event weight. In this manner, one may show, as is done in Ref. [19], that the fully decayed event weight is bounded from above by

$$\frac{d\sigma}{d(\Omega_{\text{full}})} < B_{\text{max}} \frac{d\sigma}{d(\Omega_{\text{prod}})}, \quad (2)$$

where B_{max} is a process-dependent calculable (within perturbation theory) quantity. In practice, this upper bound, denoted by r_{max} , is obtained by probing an adequate sized subsample of production PS points with decays and extracting the maximum value.

For fixed-order generation, the PS points are stored in an LHE file format, with `eventgroup` labeling the groupings of PS points which cancel in the IR regions [20]. In the top quark pair production, the PS points consist of a $2 \rightarrow 2$ configuration (we refer to these as Born PS points with subscript B , but include also virtual and soft and/or collinear counter terms), with two top quarks in the final state, and $2 \rightarrow 3$ configurations (we refer to these as real PS points, with subscript R), with top quarks plus an additional real emission particle in the final state. Let N be the number of eventgroups in the LHE production file, let $d_{B/R}$ denote the weight of the fully decayed PS point for the Born or real PS points, and $p_{B/R}$ denote similarly the weights at production stage. Schematically, the cross section for the fully decayed process σ_{dec} can then be rewritten as

$$\sigma_{\text{dec}} = \sum_{i=1}^N (d_B^i + d_R^i) = r_{\text{max}} \sum_{i=1}^N \frac{r_B^i}{r_{\text{max}}} \left(p_B^i + \frac{r_R^i}{r_B^i} p_R^i \right) \quad (3)$$

where we define the ratios $r_{B/R}^i$ as the ratios between the fully decayed and production weights,

$$r_{B/R}^i = \frac{d_{B/R}^i}{p_{B/R}^i}, \quad (4)$$

and r_{max} is the upper bound as we have defined it right after Eq. 2, obtained from the Born configurations. Now the procedure is to note that the PS point weight may be decomposed into, following notation from Ref. [21]

$$p^i = f_{1/h_1}(x_1^i, \mu_F) f_{2/h_2}(x_2^i, \mu_F) |M_{\text{prod}}^i|^2 d\Omega_i^{\text{prod}} \quad (5)$$

where $f_{i/h_j}(x, \mu_F)$ denotes the parton distribution function for parton i in hadron j at the longitudinal momentum fraction x_i at factorization scale μ_F . $|M^i|^2$ denotes the (color- and spin-summed) matrix-element squared for the given PS point and finally $d\Omega_i^{\text{prod}}$ is the corresponding phase-space factor (including flux factors) in the production final state. The fully decayed PS point weight is similarly written as

$$d^i = f_{1/h_1}(x_1^i, \mu_F) f_{2/h_2}(x_2^i, \mu_F) |M_{\text{full}}^i|^2 d\Omega_i^{\text{full}}. \quad (6)$$

Attachment of an unweighted decay PS point to a production PS point retains the same parton distribution functions and hence these cancel in the ratio

$$r^i = \frac{|M_{\text{full}}^i|^2 d\Omega_i^{\text{full}}}{|M_{\text{prod}}^i|^2 d\Omega_i^{\text{prod}}}, \quad (7)$$

where we omit the subscript B/R . The full phase space factorises into the production and decay phase space,

$$d\Omega_{\text{full}} \propto d\Omega_{\text{prod}} d\Omega_{\text{dec}}, \quad (8)$$

and for an unweighted sample of decay PS points, the decay phase space gets mapped to

$$d\Omega_{\text{dec}} \rightarrow \frac{d\Omega_{\text{dec}}}{|M_{\text{dec}}|^2}, \quad (9)$$

where we have omitted any constants including the flux factor, total branching ratio, and number of PS points. Finally, this allows us to write the reweighting ratio in Eq. 7 as

$$r^i \propto \frac{|M_{\text{full}}^i|^2}{|M_{\text{prod}}^i|^2 |M_{\text{dec}}|^2}. \quad (10)$$

For its purpose of use, in Eq. 3, in the ratio $\frac{r_R^i}{r_B^i}$ the constants drop out, leaving the relevant piece to be fully determined by the amplitudes squared of the production, fully decayed and decay PS point only as given by Eq. 10.

For exact IR pole cancellations, in the soft and collinear regions, this reweighting step must yield exactly identity factors, $\frac{r_R^i}{r_B^i} \rightarrow 1$. Due to numerical imprecision, this ratio of ratios will yield cases in which they are different from unity with a significant amount. Hence, the final cross section and distributions are prone to large statistical errors when these cancellations are not exact. To remedy this numerical inaccuracy, we introduce a smooth mapping function, which maps the ratios to the form

$$\frac{r_R^i}{r_B^i} = \begin{cases} 1 & \text{for } p_T < x_{\min} \\ 1 + D(p_T) \left(\frac{r_R^i}{r_B^i} - 1 \right) & \text{for } x_{\min} \leq p_T \leq x_{\max} \\ \frac{r_R^i}{r_B^i} & \text{for } p_T > x_{\max} \end{cases}, \quad (11)$$

where p_T is the transverse momentum of the extra emission¹. The smooth damping function $D(x)$ is chosen arbitrarily. In our calculations we use the smooth step function to third order,

$$D(x) = 3 \frac{(x - x_{\min})^2}{(x_{\max} - x_{\min})^2} - 2 \frac{(x - x_{\min})^3}{(x_{\max} - x_{\min})^3} \quad (12)$$

¹Formally this function introduces a small dependence on the FKS mapping [22, 23] for the values of $p_T < x_{\max}$. However in practice this effect is expected to be negligible.

with x_{\min}, x_{\max} chosen empirically. Thus, the values used for the calculation, $x_{\min} = 15.0$ GeV and $x_{\max} = 30.0$ GeV, were obtained by comparing a set of values and picking the two limits such that the numerical fluctuations vanish, at the same time as the interval of this soft damping $x_{\max} - x_{\min}$ is chosen to be as small as possible. It should be noted that for massless final states, the p_T of the extra emission cannot act as a proxy for the soft and collinear regions simultaneously as it does for the present case of massive top quarks. In general, one must introduce a check for all the collinear regions carefully, and in that way obtain the smooth mapping function which smoothens the boundary for the soft/collinear regions.

2.2 Spin correlation coefficients

A thorough examination of spin correlations for top quark pair production is done through the spin-density formalism [5, 24]. This introduces a set of coefficients which parameterize the cross section along different axes in some reference frame in which the spins of the top quarks are expressed. In order to present this, we must first introduce the frame of reference in which we define the leptonic angles.

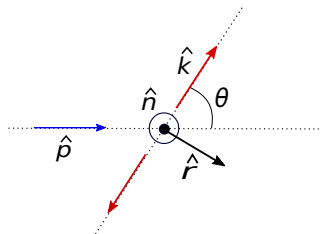


Figure 1: The orthonormal basis for the spin projections. The blue arrow indicates the direction of one of the proton beams in the laboratory frame. The red arrows indicate top and anti-top directions in the $t\bar{t}$ center of momentum frame. The angle θ defines the angle between the beam and the outgoing top quark.

One introduces a suitable orthonormal basis for the spin directions. We follow the definitions and notations used in Ref. [5]. Let \hat{k} be the direction of the top quark in the $t\bar{t}$ center of momentum frame, rotation-free boosted from the laboratory frame, and \hat{p} be the direction of motion of one of the proton beams in the laboratory frame. We then define a normal \hat{n} to the plane spanned by \hat{k} and \hat{p} and finally define a unit vector \hat{r} which completes to a right-handed orthonormal basis $\{\hat{k}, \hat{n}, \hat{r}\}$, see Fig. 1, given by

$$\begin{aligned}\hat{n} &= \text{sign}(\cos \theta) \frac{1}{\sin \theta} \hat{p} \times \hat{k}, \\ \hat{r} &= \text{sign}(\cos \theta) \frac{1}{\sin \theta} (\hat{p} - \hat{k} \cos \theta),\end{aligned}\tag{13}$$

where the $\text{sign}(\cos \theta)$ is introduced in order to maintain non-vanishing coefficients due to CP transformations [5, 25]. Then finally we are ready to define the leptonic angles in this frame,

$$\begin{aligned}\cos \theta_+^k &= \hat{p}_{\ell^+} \cdot \hat{k} & \cos \theta_-^k &= \hat{p}_{\ell^-} \cdot \hat{k} \\ \cos \theta_+^n &= \hat{p}_{\ell^+} \cdot \hat{n} & \cos \theta_-^n &= \hat{p}_{\ell^-} \cdot \hat{n} \\ \cos \theta_+^r &= \hat{p}_{\ell^+} \cdot \hat{r} & \cos \theta_-^r &= \hat{p}_{\ell^-} \cdot \hat{r},\end{aligned}\tag{14}$$

with the charged lepton directions of motion \hat{p}_{ℓ^\pm} and the angles are defined to be θ_+ for the l^+ and θ_- for the l^- . In terms of these definitions, the normalised differential distribution is expanded according to

$$\frac{1}{\sigma} \frac{d\sigma}{d \cos \theta_+^i d \cos \theta_-^j} = \frac{1}{4} (1 + B_+^i \cos \theta_+^i + B_-^j \cos \theta_-^j + C_{ij} \cos \theta_+^i \cos \theta_-^j) \quad (15)$$

for $i, j = \{\hat{k}, \hat{n}, \hat{r}\}$. This introduces a set of six B coefficients and nine C coefficients. By expansion and integration of this expression, one may extract the coefficients from a fixed-order PS point generation by the identities

$$C_{ij} = -9 \frac{\langle \cos \theta_+^i \cos \theta_-^j \rangle}{\sigma}, \quad B_{\pm}^i = 3 \frac{\langle \cos \theta_{\pm}^i \rangle}{\sigma} \quad (16)$$

in which the factors -9 and 3 are introduced to maintain correct normalisation [5].

For all coefficients $\mathcal{O} = B, C$, the perturbative expansion in the QCD coupling may be obtained via an unexpanded or an expanded expression. For both of these groups of coefficients, we may write the functional form as (absorbing in the numerator the numerical factors of 3 and -9)

$$\mathcal{O} = \frac{\sigma_{\mathcal{O}}}{\sigma} = \frac{\sigma_{\mathcal{O}, \text{NLO}}^{\text{QCD+EW}}}{\sigma_{\text{NLO}}^{\text{QCD+EW}}}. \quad (17)$$

This definition of the observables is a perturbative series in the strong coupling α_S and the electroweak coupling α . The unexpanded definition results in the evaluation of the numerator and denominator separately at the order of interest followed by the division. An expanded version corresponds to the explicit expansion in α_S of the quotient function. In the following we denote with N and D the numerator and denominator functions respectively, with the subscripts denoting the order of accuracy.

The NLO QCD accurate quotients, unexpanded, is then

$$\mathcal{O}_{\text{NLO}}^{\text{QCD}} = \frac{N_{\text{NLO}}^{\text{QCD}}}{D_{\text{NLO}}^{\text{QCD}}}. \quad (18)$$

We obtain the expanded version by expanding in α_S and neglecting terms of order $O(\alpha_S^2)$ and higher,

$$\tilde{\mathcal{O}}_{\text{NLO}}^{\text{QCD}} = K_{\text{NLO}}^{\text{QCD}} \mathcal{O}_{\text{NLO}}^{\text{QCD}} + (1 - K_{\text{NLO}}^{\text{QCD}}) \frac{N_{\text{LO}}^{\text{QCD}}}{D_{\text{LO}}^{\text{QCD}}}, \quad (19)$$

where $K_{\text{NLO}}^{\text{QCD}}$ is the inclusive NLO QCD K -factor. That is, Eq. 19 is a result of an exact α_S expansion of Eq. 18 up to NLO accuracy. We use this equation as a starting point to define the expanded $\tilde{\mathcal{O}}$ with EW corrections, assuming that their effects to both the denominator D and the inclusive K -factor are negligible. This assumption is valid since these quantities are constructed from the total cross sections. The same strategy is followed in Refs. [25, 26] for the LHC and Tevatron $t\bar{t}$ asymmetries. This results in the following expression for the complete-NLO expanded observables

$$\tilde{\mathcal{O}}_{\text{NLO}}^{\text{QCD+EW}} = K_{\text{NLO}}^{\text{QCD}} \mathcal{O}_{\text{NLO}}^{\text{QCD+EW}} + (1 - K_{\text{NLO}}^{\text{QCD}}) \frac{N_{\text{LO}}^{\text{QCD}}}{D_{\text{LO}}^{\text{QCD}}}. \quad (20)$$

Eqs. 19 and 20 are also used to extract the scale and PDF uncertainties for the expanded observables, after calculating each term for all the separate renormalisation/factorisation scale and PDF variation-member values.

2.3 Asymmetries

The top quark charge asymmetry has been previously calculated for LHC (central-peripheral) and Tevatron (forward-backward) at NNLO QCD + NLO EW in Refs. [25, 26]. In this work, we perform an evaluation of this asymmetry as a cross check of the implementation of the reweighting at fixed-order, and present novel results for the asymmetries related to the decay products. As customary, we define the rapidity (pseudorapidity) differences for the massive top pair (massless charged lepton pair) as

$$\Delta y_{tt} = |y_t| - |y_{\bar{t}}|, \quad (21)$$

$$\Delta \eta_{\ell\ell} = |\eta_{\ell^+}| - |\eta_{\ell^-}|. \quad (22)$$

We define in addition the angular differences for the lepton pair

$$\Delta \Phi_{\ell\ell} = \Phi(\ell^+) - \Phi(\ell^-), \quad (23)$$

$$\Delta \theta_{\ell\ell} = \theta(\ell^+) - \theta(\ell^-) \quad (24)$$

with $\Delta \Phi_{\ell\ell}$ being the difference of the lepton azimuthal angles in the transverse plane, and $\Delta \theta_{\ell\ell}$ the angular difference between the charged leptons in the laboratory frame. Below we define the four asymmetries which are examined in the present work.

- Top central-peripheral asymmetry:

$$A_C^{tt} = \frac{\sigma(\Delta y_{tt} > 0) - \sigma(\Delta y_{tt} < 0)}{\sigma(\Delta y_{tt} > 0) + \sigma(\Delta y_{tt} < 0)} \quad (25)$$

- Lepton central-peripheral asymmetry:

$$A_C^{\ell\ell} = \frac{\sigma(\Delta \eta_{\ell\ell} > 0) - \sigma(\Delta \eta_{\ell\ell} < 0)}{\sigma(\Delta \eta_{\ell\ell} > 0) + \sigma(\Delta \eta_{\ell\ell} < 0)} \quad (26)$$

- Lepton angular asymmetries:

$$A_{\Delta\Phi} = \frac{\sigma(|\Delta \Phi_{\ell\ell}| > \frac{\pi}{2}) - \sigma(|\Delta \Phi_{\ell\ell}| < \frac{\pi}{2})}{\sigma(|\Delta \Phi_{\ell\ell}| > \frac{\pi}{2}) + \sigma(|\Delta \Phi_{\ell\ell}| < \frac{\pi}{2})}, \quad (27)$$

$$A_{\Delta\theta} = \frac{\sigma(\cos \Delta \theta_{\ell\ell} > 0) - \sigma(\cos \Delta \theta_{\ell\ell} < 0)}{\sigma(\cos \Delta \theta_{\ell\ell} > 0) + \sigma(\cos \Delta \theta_{\ell\ell} < 0)} \quad (28)$$

Despite the fact that the numerators of the asymmetries are differently defined with respect to the numerators of the spin correlation coefficients of Sec. 2.2, as observables they are fully described by Eq. 17. Therefore the expanded and unexpanded definitions of the asymmetries are described by Eqs. 18–20. A simplification occurs in the A_C^{tt} case, since it is zero at LO QCD, therefore the second term in the expanded definitions drops out. The top quark pair central-peripheral asymmetry was previously calculated in Ref. [25] at NNLO QCD and NLO EW. We compare our results for this asymmetry obtained from the fixed-order MadSpin module. The asymmetries based on the leptonic kinematics are novel calculations at NLO QCD+EW and hence we make a quantitative comparison to our values obtained at NLO QCD.

3 Numerical setup

For the numerical calculations we use the 5-flavour scheme NNPDF3.1_NLO_luxqed PDF set [27] from the LHAPDF library [28], implementing more accurately the photon induced processes for the electroweak corrections. For the fixed-order matrix-element generation and PS point generation, MadGraph5_aMC@NLO is used. The top quarks, which are produced on-shell, are decayed with MadSpin, which utilises the tree-level decay chain, based on the NWA.

The calculation is performed for a 13 TeV center of momentum energy proton-proton collider. The process $pp \rightarrow t\bar{t} \rightarrow W^+bW^-\bar{b} \rightarrow e^+\mu^-\nu_e\bar{\nu}_\mu b\bar{b}$ is considered, without any jet requirements. In MadSpin, the fixed-order on-shell mode [29] is used for this process with the full syntax

```
set fixed_order true
set spinmode onshell
decay t > w+ b, w+ > e+ ve
decay t~ > w- b~, w- > mu- vm~
launch
```

For the renormalisation and factorisation scale central values, we use the ones introduced in Ref. [30] and also used in Ref. [9],

$$\mu_R^0 = \mu_F^0 = \frac{H_T}{4} = \frac{\sum_i m_{T,i}}{4}, \{i = t, \bar{t}\}. \quad (29)$$

For the scale variation, the conventional 9-point envelope of $\{\frac{1}{2}\mu_{R,F}^0, 2\mu_{R,F}^0\}$ is used. The input masses are

$$\begin{aligned} m_Z &= 91.1876 \text{ GeV}, \quad m_W = 80.385 \text{ GeV}, \\ m_H &= 125 \text{ GeV}, \quad m_t = 172.5 \text{ GeV}. \end{aligned} \quad (30)$$

The widths used are calculated internally by MadSpin, with the values entering the calculations being²

$$\begin{aligned} \Gamma_Z &= 2.44412 \text{ GeV}, \quad \Gamma_W = 2.04542 \text{ GeV}, \\ \Gamma_H &= 4.07468 \text{ MeV}, \quad \Gamma_t = 1.48060 \text{ GeV}. \end{aligned} \quad (31)$$

We utilise the G_μ renormalisation scheme in which we use the EW parameters:

$$G_\mu = 1.166379 \times 10^{-5} \text{ GeV}^{-2} \iff \alpha_{\text{EW}} = 1/132.2332. \quad (32)$$

4 Results

We move now into presenting our results on the spin correlation coefficients, the asymmetries and the differential distributions.

²These widths are computed at LO accuracy, consistent with the fact that MadSpin includes the decays at leading order.

	Unexpanded			Expanded		
	LO QCD [%]	NLO QCD [%]	NLO QCD+EW [%]	NLO QCD [%]	NLO QCD+EW [%]	
B_k^+	0.01(2) ^{+3.7%} _{-5.0%} ^{+9.8%} _{-9.8%}	-0.001(20) ^{+0%} _{-0%} ^{+0%} _{-0%}	-0.10(3) ^{+12.0%} _{-11.9%} ^{+2.8%} _{-2.8%}	-0.006(40) ^{+0%} _{-0%} ^{+0%} _{-0%}	-0.14(5) ^{+25.5%} _{-28.1%} ^{+2.8%} _{-2.8%}	
B_n^+	-0.04(2) ^{+1.5%} _{-1.4%} ^{+4.3%} _{-4.3%}	-0.03(2) ^{+42.4%} _{-31.5%} ^{+1.6%} _{-1.6%}	0.07(4) ^{+73.0%} _{-47.6%} ^{+2.5%} _{-2.5%}	-0.03(4) ^{+54.9%} _{-44.1%} ^{+1.5%} _{-1.5%}	0.12(6) ^{+42.0%} _{-32.8%} ^{+2.5%} _{-2.5%}	
B_r^+	0.003(20) ^{+15.1%} _{-16.6%} ^{+2.0%} _{-2.0%}	-0.04(2) ^{+55.4%} _{-62.5%} ^{+4.2%} _{-4.2%}	-0.11(4) ^{+14.5%} _{-18.3%} ^{+2.0%} _{-2.0%}	-0.06(4) ^{+40.3%} _{-38.3%} ^{+3.2%} _{-3.2%}	-0.15(6) ^{+14.6%} _{-14.6%} ^{+2.1%} _{-2.1%}	
B_k^-	0.01(2) ^{+8.6%} _{-9.2%} ^{+16.5%} _{-16.5%}	0.04(2) ^{+47.9%} _{-31.5%} ^{+4.7%} _{-4.7%}	-0.13(3) ^{+9.4%} _{-11.3%} ^{+7.3%} _{-7.3%}	0.05(4) ^{+39.5%} _{-31.8%} ^{+4.7%} _{-4.7%}	-0.18(5) ^{+16.8%} _{-20.5%} ^{+8.1%} _{-8.1%}	
B_n^-	-0.07(2) ^{+1.0%} _{-0.7%} ^{+0.9%} _{-0.9%}	-0.05(2) ^{+23.3%} _{-18.6%} ^{+2.5%} _{-2.5%}	-0.05(4) ^{+35.9%} _{-49.1%} ^{+2.2%} _{-2.2%}	-0.04(4) ^{+36.8%} _{-35.1%} ^{+3.4%} _{-3.4%}	-0.04(6) ^{+88.0%} _{-100.2%} ^{+2.4%} _{-2.4%}	
B_r^-	-0.01(2) ^{+7.1%} _{-7.4%} ^{+0.6%} _{-0.6%}	-0.02(2) ^{+26.9%} _{-32.5%} ^{+3.0%} _{-3.0%}	-0.13(4) ^{+13.5%} _{-26.1%} ^{+2.6%} _{-2.6%}	-0.02(4) ^{+22.9%} _{-26.3%} ^{+2.0%} _{-2.0%}	-0.17(6) ^{+9.3%} _{-13.9%} ^{+3.7%} _{-3.7%}	

Table 1: The B coefficients as defined in Eq. 16 at various orders both expanded and unexpanded.

	Unexpanded			Expanded		
	LO QCD [%]	NLO QCD [%]	NLO QCD+EW [%]	NLO QCD [%]	NLO QCD+EW [%]	
C_{kk}	32.68(3) ^{+1.5%} _{-1.7%} ^{+0.8%} _{-0.8%}	32.88(3) ^{+1.3%} _{-0.4%} ^{+0.7%} _{-0.7%}	32.69(5) ^{+1.1%} _{-0.4%} ^{+0.7%} _{-0.7%}	32.96(7) ^{+1.7%} _{-0.8%} ^{+0.6%} _{-0.6%}	32.65(9) ^{+1.5%} _{-0.6%} ^{+0.6%} _{-0.6%}	
C_{nn}	33.01(3) ^{+0.3%} _{-0.5%} ^{+0.2%} _{-0.2%}	31.97(3) ^{+0.9%} _{-1.1%} ^{+0.2%} _{-0.2%}	31.89(5) ^{+0.9%} _{-1.3%} ^{+0.2%} _{-0.2%}	31.59(7) ^{+0.6%} _{-0.5%} ^{+0.2%} _{-0.2%}	31.49(9) ^{+0.7%} _{-0.6%} ^{+0.2%} _{-0.2%}	
C_{rr}	0.71(3) ^{+45.1%} _{-51.5%} ^{+3.2%} _{-3.2%}	4.80(3) ^{+28.9%} _{-19.2%} ^{+2.8%} _{-2.8%}	4.83(5) ^{+29.4%} _{-19.4%} ^{+2.5%} _{-2.5%}	6.28(7) ^{+12.6%} _{-8.3%} ^{+1.9%} _{-1.9%}	6.33(9) ^{+11.6%} _{-8.1%} ^{+1.7%} _{-1.7%}	
$C_{nr} + C_{rn}$	-0.02(4) ^{+18.4%} _{-18.8%} ^{+1.0%} _{-1.0%}	0.002(50) ^{+0%} _{-0%} ^{+0%} _{-0%}	0.08(7) ^{+60.6%} _{-59.7%} ^{+3.8%} _{-3.8%}	0.01(10) ^{+0%} _{-0%} ^{+0%} _{-0%}	0.1(1) ^{+45.2%} _{-48.4%} ^{+3.6%} _{-3.6%}	
$C_{nr} - C_{rn}$	0.02(4) ^{+10.5%} _{-12.0%} ^{+1.8%} _{-1.8%}	-0.05(4) ^{+29.9%} _{-53.6%} ^{+4.0%} _{-4.0%}	-0.08(7) ^{+34.1%} _{-54.3%} ^{+8.3%} _{-8.3%}	-0.07(9) ^{+22.1%} _{-31.6%} ^{+2.4%} _{-2.4%}	-0.1(1) ^{+23.0%} _{-28.3%} ^{+7.5%} _{-7.5%}	
$C_{nk} + C_{kn}$	-0.02(4) ^{+13.1%} _{-10.3%} ^{+3.3%} _{-3.3%}	-0.004(60) ^{+0%} _{-0%} ^{+0%} _{-0%}	-0.14(9) ^{+30.8%} _{-40.6%} ^{+5.1%} _{-5.1%}	0.001(100) ^{+0%} _{-0%} ^{+0%} _{-0%}	-0.2(2) ^{+28.6%} _{-30.3%} ^{+5.7%} _{-5.7%}	
$C_{nk} - C_{kn}$	-0.004(40) ^{+54.1%} _{-59.2%} ^{+3.3%} _{-3.3%}	-0.03(6) ^{+79.7%} _{-80.1%} ^{+13.9%} _{-13.9%}	0.12(9) ^{+13.7%} _{-11.4%} ^{+4.0%} _{-4.0%}	-0.04(10) ^{+78.4%} _{-83.5%} ^{+9.3%} _{-9.3%}	0.2(2) ^{+6.5%} _{-8.3%} ^{+4.1%} _{-4.1%}	
$C_{rk} + C_{kr}$	-22.87(4) ^{+1.5%} _{-1.5%} ^{+0.4%} _{-0.4%}	-20.51(6) ^{+3.8%} _{-2.8%} ^{+0.4%} _{-0.4%}	-20.48(9) ^{+4.1%} _{-2.9%} ^{+0.4%} _{-0.4%}	-19.7(1) ^{+2.3%} _{-1.4%} ^{+0.3%} _{-0.3%}	-19.6(1) ^{+2.2%} _{-1.5%} ^{+0.4%} _{-0.4%}	
$C_{rk} - C_{kr}$	0.02(4) ^{+17.2%} _{-15.7%} ^{+5.1%} _{-5.1%}	-0.13(6) ^{+18.1%} _{-30.7%} ^{+2.2%} _{-2.2%}	0.09(9) ^{+52.4%} _{-29.4%} ^{+4.7%} _{-4.7%}	-0.2(1) ^{+10.2%} _{-13.1%} ^{+2.2%} _{-2.2%}	0.1(2) ^{+36.8%} _{-25.0%} ^{+4.8%} _{-4.8%}	

Table 2: The C coefficients as defined in Eq. 16 at various orders both expanded and unexpanded.

Correlation coefficients

We start with the Tabs. 1, 2, where we show the B and C spin correlation coefficients respectively. For the NLO QCD and the complete-NLO calculations we present the results from both the unexpanded and expanded definitions. In all cases we show the absolute statistical error and the relative scale and PDF uncertainties.

In Tab. 1 we see that almost all of the coefficients are compatible with zero at LO and NLO QCD accuracy for both the unexpanded and expanded definitions. At the complete-NLO accuracy there is a small deviation from zero for some coefficients. In Tab. 2 for the C coefficients, we find a similar trend for the coefficients being close to zero at LO, and remaining close to zero for most of the coefficients, except the C_{kk} , C_{nn} , C_{rr} , $C_{rk} + C_{kr}$ also at NLO QCD. For the vanishing C coefficients, they remain compatible with zero also when the complete-NLO corrections are considered, in contrast to some of the B coefficients which obtain a finite correction. For the four non-zero coefficients, the EW corrections are small and do not alter the NLO QCD prediction. They further show stability between the unexpanded and expanded predictions.

In our calculation we do not include the NLO corrections to the top quark decays and the spin correlations from the virtual part of the NLO in the $t\bar{t}$ production. These effects can be evaluated by comparison of the results in Ref. [15], which include NLO QCD corrections in both the production and decay, to the results obtained via MCFM based on Ref. [18], where the decay is included at LO. We list in Tab. 3 the values from Ref. [15], and the results one obtains from the MCFM implementation for the four non-zero spin correlation coefficients.

As can be seen from this table, the NLO QCD corrections in the decay do not affect

QCD order / [%]	C_{kk}	C_{nn}	C_{rr}	C_{rk+kr}
NLO \times NLO ([15])	33.0(3)	33.0(2)	5.8(2)	-20.3(2)
NLO \times LO (MCFM)	33.04(4)	33.09(4)	5.96(4)	-20.71(7)

Table 3: The four largest spin correlation coefficients at NLO in decay (from Ref. [15]) and with LO in decay based on the MCFM parton-level process library.

Asymmetry	LO QCD [%]	Unexpanded			Expanded		
		NLO QCD [%]	NLO QCD+EW [%]	NLO QCD [%]	NLO QCD+EW [%]		
A_C^{tt}	0	0.453(5) ^{+28.2% +3.4%} _{-20.5% -3.4%}	0.546(6) ^{+25.1% +2.4%} _{-18.0% -2.4%}	0.62(2) ^{+18.1% +3.3%} _{-14.8% -3.3%}	0.73(3) ^{+13.8% +2.3%} _{-11.5% -2.3%}		
$A_C^{\ell\ell}$	0	0.27(2) ^{+29.3% +3.8%} _{-21.4% -3.8%}	0.33(3) ^{+25.0% +3.8%} _{-17.8% -3.8%}	0.36(3) ^{+19.3% +3.7%} _{-15.9% -3.7%}	0.45(4) ^{+14.6% +3.9%} _{-12.0% -3.9%}		
$A_{\Delta\Phi}$	17.51(1) ^{+3.2% +0.4%} _{-2.8% -0.4%}	12.65(2) ^{+8.3% +0.4%} _{-14.8% -0.4%}	12.42(3) ^{+8.7% +0.4%} _{-15.5% -0.4%}	10.88(3) ^{+7.2% +0.3%} _{-10.1% -0.3%}	10.58(4) ^{+7.4% +0.4%} _{-10.5% -0.4%}		
$A_{\Delta\theta}$	14.63(1) ^{+4.0% +1.5%} _{-4.6% -1.5%}	16.03(2) ^{+4.0% +1.4%} _{-2.2% -1.4%}	16.24(2) ^{+4.1% +1.4%} _{-2.2% -1.4%}	16.54(3) ^{+2.9% +1.3%} _{-1.7% -1.3%}	16.83(4) ^{+2.8% +1.3%} _{-1.5% -1.3%}		

Table 4: Asymmetries at various orders as defined in Sec. 2.3, both expanded and unexpanded.

these spin correlation coefficients. This allows a safe conclusion that our results for the spin correlations with complete NLO in production and LO in decay should not be greatly altered if one includes also the NLO QCD in the decay. The differences between the coefficients obtained with MCFM in Tab. 3 and our corresponding results in Tab. 2 is of the order of percent level with the exception of the C_{rr} , where they are at $\sim 25\%$. The origin of these differences are the virtual spin corrections, which are approximated with the tree-level ones in our calculation, but are included in the MCFM calculation. Both the results obtained via MCFM and the results in Ref. [15] agree with our results regarding the spin correlation coefficients that are compatible with zero.

Asymmetries

Moving to the asymmetries shown in Tab. 4, in the first line we show the already known A_C^{tt} , which is in agreement with the results obtained from the $t\bar{t}$ production asymmetry study [25] for the corresponding orders at 13 TeV. We further present the dilepton asymmetries as defined in Sec. 2.3. The $A_C^{\ell\ell}$ is smaller in comparison to the A_C^{tt} at all perturbative orders, and the complete NLO has a similar effect, an increase of $\sim 20\%$ for both of the asymmetries as compared to the NLO QCD. The $A_{\Delta\Phi}$, $A_{\Delta\theta}$ are non-zero already at LO QCD. For the $A_{\Delta\Phi}$ the NLO QCD corrections reduce the asymmetry and the EW ones further reduce it but by a smaller amount. The $A_{\Delta\theta}$ behaves in the opposite way regarding the higher order corrections. In both cases the expanded definitions behave accordingly.

Differential distributions

Regarding the top quark pair distributions ($p_T(t)$, $m(t\bar{t})$, $y(t)$) we have checked that in our results the effects of the EW corrections are in agreement with the results presented in Ref. [31].

For the decay level differential distributions we focus on the leptons. We show the normalised leptonic distributions in Figs. 2, 3, since they significantly reduce the theoretical uncertainties as well as the systematic experimental errors with respect to the unnormalised ones. In all cases we show the LO QCD, NLO QCD and NLO QCD+EW distributions. In the first inset we show the ratio between the NLO QCD and LO QCD normalised differential distributions. In the second inset we present the NLO QCD+EW over the NLO QCD one.

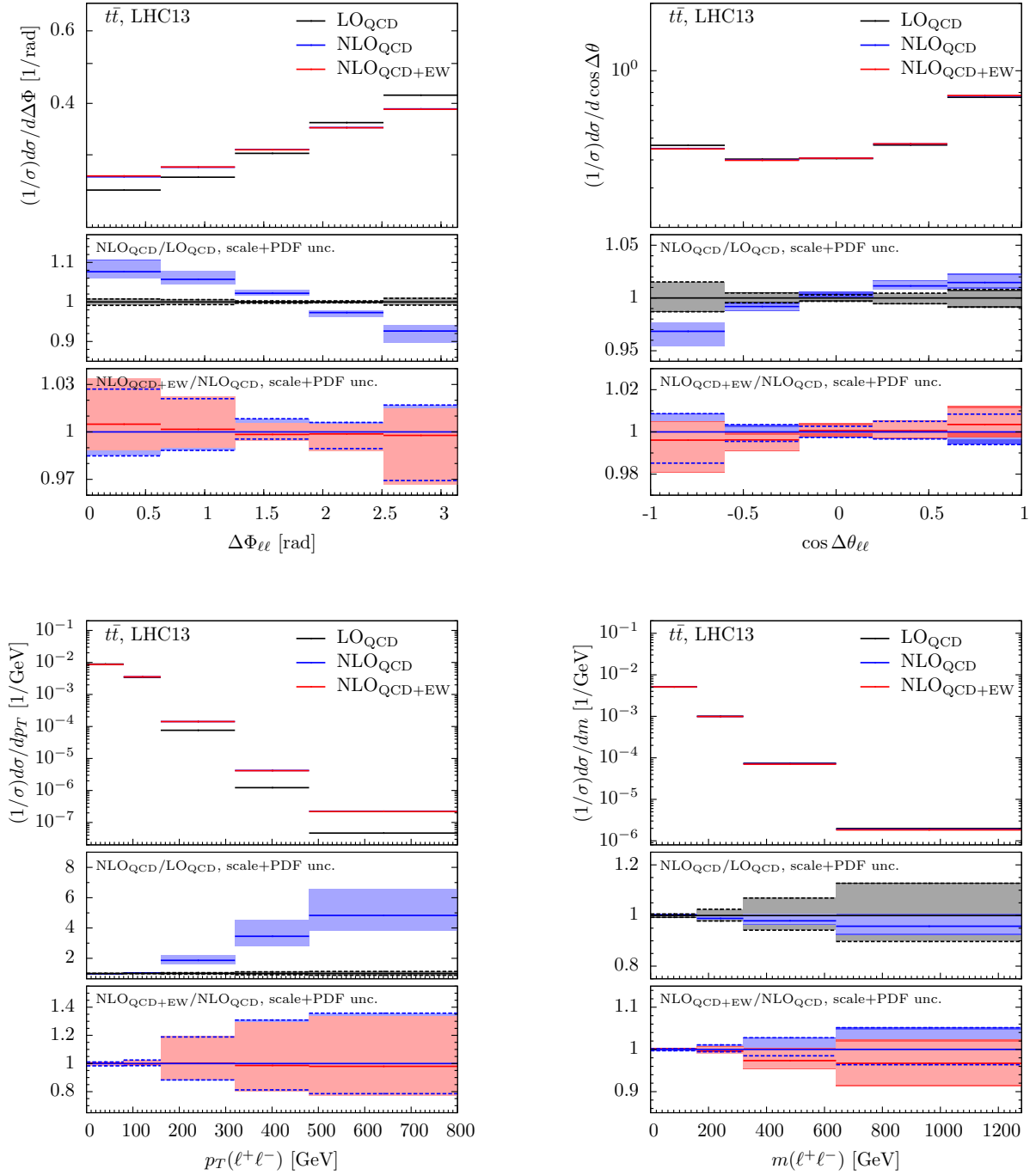


Figure 2: The $\Delta\Phi_{\ell\ell}$ distribution (upper left) and $\cos \Delta\theta_{\ell\ell}$ distributions (upper right), transverse momentum of $\ell^+\ell^-$ system (lower left) and dilepton invariant mass distribution (lower right).

In both insets we show the scale and PDF uncertainties for all the predictions. In all cases the scale uncertainties are the light-coloured band around the central value and the added PDF uncertainties in quadrature to the scale ones are the dark-coloured band. We start our discussion with the lepton pair angular distributions $\Delta\Phi_{\ell\ell}$ and $\cos \Delta\theta_{\ell\ell}$ in Fig. 2 (upper plots), which are directly connected to the corresponding asymmetries presented in Tab. 4. In the first inset of the $\Delta\Phi_{\ell\ell}$ and $\cos \Delta\theta_{\ell\ell}$ plots we see the large effect of the QCD corrections. Furthermore the shape of the QCD corrections is in agreement with the reduction and increase of the $A_{\Delta\Phi}$ and $A_{\Delta\theta}$ respectively, as shown in Tab. 4, since the dilepton asymmetries $A_C^{\ell\ell}, A_{\Delta\Phi}, A_{\Delta\theta}$ are fully correlated to the leptonic differential distributions $\eta(\ell), \Delta\Phi_{\ell\ell}$ and $\cos \Delta\theta_{\ell\ell}$. In the second

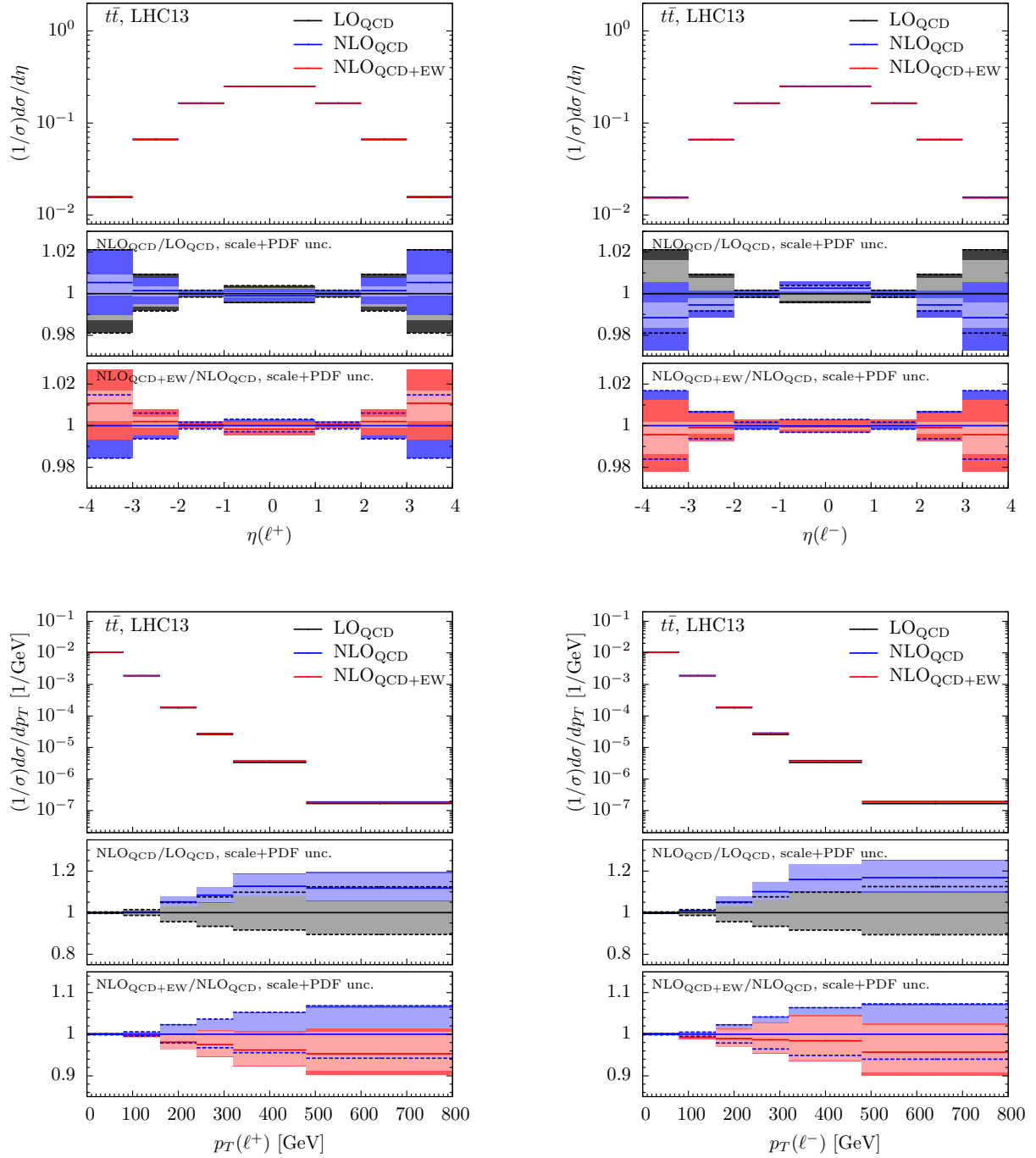


Figure 3: Pseudorapidity (upper) and transverse momentum (lower) lepton distributions.

inset of these plots we see the small effect (below one percent) of the EW corrections in both distributions.

We continue the description of the lepton pair by showing the invariant mass and the transverse mass of the system in Fig. 2 (lower plots). In the $p_T(\ell^+\ell^-)$ we firstly observe the very large effect of the NLO QCD corrections, a giant K -factor appearing in the highly cross-section suppressed tail, which is already known [15], and secondly that the effect of the EW corrections is negligible for this distribution. Moving to the $m(\ell^+\ell^-)$ distribution we see an EW effect of $\sim 2\%$ below 500 GeV and of $\sim 5\%$ after 500 GeV. The $m(\ell^+\ell^-)$ spectrum is softened with respect to the NLO QCD prediction. The effect lies along the lower band of the NLO QCD

normalised uncertainties, but given the fact that the QCD predictions have reached the NNLO accuracy [15] with the scale uncertainty being decreased to a few percent level, the EW corrections will alter the prediction for this observable. For the distributions shown in Fig. 2 the PDF uncertainties are very small to negligible w.r.t. the scale uncertainties.

Regarding the separate lepton distributions we show the pseudorapidities and the transverse momenta of the leptons emerging from top quark pair in Fig. 3. In the pseudorapidity distributions (upper plots) we see in the first insets the non-zero NLO QCD induced lepton asymmetry, which is also shown in Tab. 4. In the second insets we see the enhancement of this feature due to the EW corrections, but in both cases these effects are below $\sim 2\%$ and appear at large rapidity regimes ($|\eta| > 3$). From the shape of the ratio insets we can see that the observed effects from both the QCD and EW corrections will cancel in the case of an averaged $\eta(\ell)$ distribution. In the transverse momentum distributions (lower plots) we see the large positive effect of the NLO QCD corrections in the first inset. In the second inset we observe that the EW effects become negative at higher p_T values reaching a negative correction of $\sim 5\%$ with respect to the NLO QCD prediction between 500 and 800 GeV. In the case of the lepton p_T 's as well as the $m(\ell^+\ell^-)$ the EW corrections bring the predictions closer to the data at the tails, according to the comparisons between NNLO QCD predictions and experimental results in Ref. [15]. The high $|\eta(\ell)|$ regimes show scale and PDF uncertainties of the same level, whereas the theory uncertainties of the $p_T(\ell)$ distributions are fully dominated by the scale variation. Our results concerning the $\Delta\Phi_{\ell\ell}$, $\cos\Delta\theta_{\ell\ell}$ and $p_T(\ell)$ distributions are qualitatively similar to what has been found in Ref. [13], where part of the NLO EW corrections is included.

5 Conclusion and discussion

In this work we have presented for the first time the complete-NLO corrections of the $t\bar{t}$ production to the spin correlation coefficients, the leptonic asymmetries and the differential leptonic distributions. We have focused on the process of top quark pair production and decay to a dilepton channel at fixed-order. We tested our method for the reweighting at fixed-order by comparing the $t\bar{t}$ asymmetry and top quark distributions to already known results and found that they are in good agreement.

Our calculation has two major approximations: firstly, we consider the tree-level spin correlations. This was investigated by comparison to available results in the literature to find that one of the four dominant spin-correlation coefficients obtain a sizeable difference, while the other coefficients are insensitive to the virtual spin correlations. Secondly, we use an accuracy of electroweak precision in the production, while keeping a LO precision in the decay. Despite these approximations, the present results indicate the size of the electroweak effects.

We investigated in particular the effects on the spin correlation in terms of the expansion coefficients within the spin-density formalism. We found that the EW effects, now included in the complete NLO, have very small effect compared to the NLO QCD results on most of the spin correlation coefficients. However, for some coefficients the contribution moves the result from zero to a finite value. We investigated the coefficients both expanded and unexpanded in the strong coupling, and found similar effects of the complete NLO in both versions. We further investigated the asymmetries, both those which have been known from previous calculations (the $t\bar{t}$ central-peripheral asymmetry) and the leptonic asymmetries calculated for the first time at this accuracy. We found there that the EW effects are present with a few percent effect. Finally we have studied the normalised leptonic differential distributions. We found that in specific phase-space regions of the transverse momentum and invariant mass distributions the

complete-NLO calculation softens the NLO QCD prediction by a few percent, lying close to the lower border of the NLO QCD uncertainty band.

Acknowledgements

We thank Olivier Mattelaer for discussions regarding MadSpin. IT would like to thank Eleni Vryonidou for useful discussions on the spin correlation coefficient definitions. This work is done in the context of and supported by the Swedish Research Council under contract number 2016-05996. The work of IT is also supported by the MorePheno ERC grant agreement under number 668679. Computational resources to IT have been provided by the Consortium des Équipements de Calcul Intensif (CÉCI), funded by the Fonds de la Recherche Scientifique de Belgique (F.R.S.-FNRS) under Grant No. 2.5020.11 and by the Walloon Region.

References

- [1] W. Bernreuther, A. Brandenburg, Z. G. Si, and P. Uwer, “Spin properties of top quark pairs produced at hadron colliders,” *Acta Phys. Polon. B*, vol. 34, pp. 4477–4490, 2003, hep-ph/0304244.
- [2] W. Bernreuther, A. Brandenburg, Z. G. Si, and P. Uwer, “Top quark spin correlations at hadron colliders: Predictions at next-to-leading order QCD,” *Phys. Rev. Lett.*, vol. 87, p. 242002, 2001, hep-ph/0107086.
- [3] W. Bernreuther, A. Brandenburg, Z. G. Si, and P. Uwer, “Next-to-leading order QCD corrections to top quark spin correlations at hadron colliders: The Reactions $gg \rightarrow t \text{ anti-}t(g)$ and $gq(\text{anti-}q) \rightarrow t \text{ anti-}tq(\text{anti-}q)$,” *Phys. Lett. B*, vol. 509, pp. 53–58, 2001, hep-ph/0104096.
- [4] W. Bernreuther and Z.-G. Si, “Top quark spin correlations and polarization at the LHC: standard model predictions and effects of anomalous top chromo moments,” *Phys. Lett. B*, vol. 725, pp. 115–122, 2013, 1305.2066. [Erratum: *Phys.Lett.B* 744, 413–413 (2015)].
- [5] W. Bernreuther, D. Heisler, and Z.-G. Si, “A set of top quark spin correlation and polarization observables for the LHC: Standard Model predictions and new physics contributions,” *JHEP*, vol. 12, p. 026, 2015, 1508.05271.
- [6] M. Aaboud *et al.*, “Measurements of top quark spin observables in $t\bar{t}$ events using dilepton final states in $\sqrt{s} = 8$ TeV pp collisions with the ATLAS detector,” *JHEP*, vol. 03, p. 113, 2017, 1612.07004.
- [7] A. M. Sirunyan *et al.*, “Measurement of the top quark polarization and $t\bar{t}$ spin correlations using dilepton final states in proton-proton collisions at $\sqrt{s} = 13$ TeV,” *Phys. Rev. D*, vol. 100, no. 7, p. 072002, 2019, 1907.03729.
- [8] G. Aad *et al.*, “Measurement of the $t\bar{t}$ production cross-section and lepton differential distributions in $e\mu$ dilepton events from pp collisions at $\sqrt{s} = 13$ TeV with the ATLAS detector,” *Eur. Phys. J. C*, vol. 80, no. 6, p. 528, 2020, 1910.08819.
- [9] A. Behring, M. Czakon, A. Mitov, A. S. Papanastasiou, and R. Poncelet, “Higher order corrections to spin correlations in top quark pair production at the LHC,” *Phys. Rev. Lett.*, vol. 123, no. 8, p. 082001, 2019, 1901.05407.

- [10] K. Melnikov and M. Schulze, “NLO QCD corrections to top quark pair production and decay at hadron colliders,” *JHEP*, vol. 08, p. 049, 2009, 0907.3090.
- [11] A. Denner and M. Pellen, “Off-shell production of top-antitop pairs in the lepton+jets channel at NLO QCD,” *JHEP*, vol. 02, p. 013, 2018, 1711.10359.
- [12] T. Ježo, J. M. Lindert, P. Nason, C. Oleari, and S. Pozzorini, “An NLO+PS generator for $t\bar{t}$ and Wt production and decay including non-resonant and interference effects,” *Eur. Phys. J. C*, vol. 76, no. 12, p. 691, 2016, 1607.04538.
- [13] A. Denner and M. Pellen, “NLO electroweak corrections to off-shell top-antitop production with leptonic decays at the LHC,” *JHEP*, vol. 08, p. 155, 2016, 1607.05571.
- [14] A. M. Sirunyan *et al.*, “Measurements of $t\bar{t}$ differential cross sections in proton-proton collisions at $\sqrt{s} = 13$ TeV using events containing two leptons,” *JHEP*, vol. 02, p. 149, 2019, 1811.06625.
- [15] M. Czakon, A. Mitov, and R. Poncelet, “NNLO QCD corrections to leptonic observables in top-quark pair production and decay,” *JHEP*, vol. 05, p. 212, 2021, 2008.11133.
- [16] R. Frederix, S. Frixione, V. Hirschi, D. Pagani, H. S. Shao, and M. Zaro, “The automation of next-to-leading order electroweak calculations,” *JHEP*, vol. 07, p. 185, 2018, 1804.10017.
- [17] P. Artoisenet, R. Frederix, O. Mattelaer, and R. Rietkerk, “Automatic spin-entangled decays of heavy resonances in Monte Carlo simulations,” *JHEP*, vol. 03, p. 015, 2013, 1212.3460.
- [18] J. M. Campbell and R. K. Ellis, “Top-Quark Processes at NLO in Production and Decay,” *J. Phys. G*, vol. 42, no. 1, p. 015005, 2015, 1204.1513.
- [19] S. Frixione, E. Laenen, P. Motylinski, and B. R. Webber, “Angular correlations of lepton pairs from vector boson and top quark decays in Monte Carlo simulations,” *JHEP*, vol. 04, p. 081, 2007, hep-ph/0702198.
- [20] J. M. Butterworth *et al.*, “THE TOOLS AND MONTE CARLO WORKING GROUP Summary Report from the Les Houches 2009 Workshop on TeV Colliders,” in *6th Les Houches Workshop on Physics at TeV Colliders*, 3 2010, 1003.1643.
- [21] O. Mattelaer, “On the maximal use of Monte Carlo samples: re-weighting events at NLO accuracy,” *Eur. Phys. J. C*, vol. 76, no. 12, p. 674, 2016, 1607.00763.
- [22] R. Frederix, S. Frixione, F. Maltoni, and T. Stelzer, “Automation of next-to-leading order computations in QCD: The FKS subtraction,” *JHEP*, vol. 10, p. 003, 2009, 0908.4272.
- [23] S. Frixione, Z. Kunszt, and A. Signer, “Three jet cross-sections to next-to-leading order,” *Nucl. Phys. B*, vol. 467, pp. 399–442, 1996, hep-ph/9512328.
- [24] W. Bernreuther and A. Brandenburg, “Tracing CP violation in the production of top quark pairs by multiple TeV proton proton collisions,” *Phys. Rev. D*, vol. 49, pp. 4481–4492, 1994, hep-ph/9312210.
- [25] M. Czakon, D. Heymes, A. Mitov, D. Pagani, I. Tsinikos, and M. Zaro, “Top-quark charge asymmetry at the LHC and Tevatron through NNLO QCD and NLO EW,” *Phys. Rev. D*, vol. 98, no. 1, p. 014003, 2018, 1711.03945.

- [26] M. Czakon, P. Fiedler, and A. Mitov, “Resolving the Tevatron Top Quark Forward-Backward Asymmetry Puzzle: Fully Differential Next-to-Next-to-Leading-Order Calculation,” *Phys. Rev. Lett.*, vol. 115, no. 5, p. 052001, 2015, 1411.3007.
- [27] V. Bertone, S. Carrazza, N. P. Hartland, and J. Rojo, “Illuminating the photon content of the proton within a global PDF analysis,” *SciPost Phys.*, vol. 5, no. 1, p. 008, 2018, 1712.07053.
- [28] A. Buckley, J. Ferrando, S. Lloyd, K. Nordström, B. Page, M. Rüfenacht, M. Schönherr, and G. Watt, “LHAPDF6: parton density access in the LHC precision era,” *Eur. Phys. J. C*, vol. 75, p. 132, 2015, 1412.7420.
- [29] O. Mattelaer, M. Mitra, and R. Ruiz, “Automated Neutrino Jet and Top Jet Predictions at Next-to-Leading-Order with Parton Shower Matching in Effective Left-Right Symmetric Models,” 10 2016, 1610.08985.
- [30] M. Czakon, D. Heymes, and A. Mitov, “Dynamical scales for multi-TeV top-pair production at the LHC,” *JHEP*, vol. 04, p. 071, 2017, 1606.03350.
- [31] M. Czakon, D. Heymes, A. Mitov, D. Pagani, I. Tsinikos, and M. Zaro, “Top-pair production at the LHC through NNLO QCD and NLO EW,” *JHEP*, vol. 10, p. 186, 2017, 1705.04105.